The Relationship between Aircraft Icing and Synoptic-Scale Weather Conditions

BEN C. BERNSTEIN, TIFFANY A. OMERON, FRANK MCDONOUGH, AND MARCIA K. POLITOVICH

Research Applications Program, National Center for Atmospheric Research, Boulder, Colorado

(Manuscript received 16 April 1996, in final form 12 May 1997)

ABSTRACT

More than 2700 aircraft icing pilot reports are compared to analyses of operationally available data for 37 cases of winter weather. Statistical results regarding the number of occurrences of icing reports with airmass origin, location relative to fronts, troughs and low pressure centers, precipitation type, cloud cover, lightning/thunder, fog, radar reflectivity, and synoptic-scale forcing mechanisms are developed. Statistics are created for several combinations of icing severity and type, including a category for some of the worst icing encountered by aircraft (clear or mixed icing of moderate or greater severity), then normalized by the areal extent of the weather features. Results indicate that the locations most conducive to icing conditions were arctic, West Coast, and East Coast air masses; 250–600 km ahead of active and stationary warm fronts; in areas of freezing drizzle, freezing rain, and ice pellets when precipitation was occurring; and in areas with obscured and overcast sky conditions when precipitation was not occurring. Icing conditions were also associated with overrunning conditions and troughs analyzed on upper-air charts. Conditions in some of these locations were conducive to the formation of large supercooled water droplets, which have recently been shown to be related to hazardous icing conditions.

1. Introduction

Flight in icing conditions is a known hazard to aircraft and has been the subject of recent field programs [e.g., the Winter Icing and Storms Project (WISP), Rasmussen et al. (1992); the Canadian Atlantic Storms Program, Stewart (1991)]. These programs have focused on the conditions that are conducive to the formation, existence, and depletion of supercooled liquid water (SLW; Rasmussen et al. 1995; Cober et al. 1995), and their effect on research aircraft (Politovich and Bernstein 1995; Politovich 1996). While these studies have shed new light on the mechanisms that create SLW, little recent information is available regarding where icing tends to form relative to synoptic-scale weather patterns. For such information, pilots and icing forecasters must rely heavily on operations handbooks, forecasters' guides, and technical memoranda, primarily based upon accumulated non-research-quality flight data and reports from the 1940s and 1950s (e.g., Air Weather Service 1980). These publications provide general guidelines for the severity and type of icing that can be expected within several portions of frontal weather systems, air masses of different origin, precipitation types, and cloud types. A significant portion of the data used to develop the guidelines was derived empirically and not substantiated by strong statistical evidence. According to Lewis (1951), the data used in those studies were ''inadequate to determine the frequency and severity of icing conditions to be expected in various areas under the influence of various synoptic situations.''

Modern in-flight icing forecasters at the Aviation Weather Center (AWC) prepare their forecasts with the help of model-based icing algorithms, such as those developed by Forbes et al. (1993), Bernstein (1996), and McCann (1997). However, even with the implementation of these tools and the availability of more sophisticated forecast models and improved satellite and radar data, forecasters still perform detailed hand analyses of the synoptic-scale weather patterns using surface and upper-air charts. Such analysis is necessary for the forecaster to understand the physical causes for the icing and to interpret the output from automated icing algorithms.

This study was undertaken in an effort to improve upon the information available in the Air Weather Service Forecaster's Guide and to provide statistical information that relates to the daily analysis that icing forecasters perform. Operationally available data from the National Centers for Environmental Prediction (NCEP), including surface, upper-air, Geostationary Operational Environmental Satellite (GOES) visible satellite, radar mosaic, lightning detection network, and daily snow cover maps were compared to pilot reports of icing (PIREPs) for 37 cases of winter and fall weather over the United States. The observations were hand analyzed, and all portions of the surface charts were tagged for

Corresponding author address: Ben C. Bernstein, NCAR, P.O. Box 3000, Boulder, CO 80307-3000.
E-mail: bernstei@rap.ucar.edu

their airmass origin, precipitation type, and location relative to surface weather features. Upper-air maps were tagged for the synoptic-scale forcing mechanisms operating in each area.

Forbes et al. (1993) performed a similar study, comparing pilot reports to surface and upper-air charts, sounding data from the National Weather Service (NWS), and the STORM-FEST field program and output from an early nonoperational version of NCEP's Eta Model (Messinger et al. 1988). That study was limited to data from February to March 1992 and focused on temperature and relative humidity thresholds derived from proximity soundings. The intent of their study was to determine if substantial numbers of icing reports were occurring beneath cold pockets or cold advection aloft that may have caused the icing to be associated with convective cells rising into otherwise dry large-scale conditions. Their results were not normalized to account for the large variation in area covered by features related to icing.

In this paper, the physical relationships between icing and synoptic-scale weather phenomena are discussed and regions within synoptic-scale weather patterns where icing conditions tended to form are identified. An improved understanding of the physical relationships between synoptic-scale weather patterns and the occurrence of icing can only serve to improve icing forecasts and the concepts used in automated icing forecast algorithms.

2. Methodology

The techniques used to calculate the statistics in this study are critical to the understanding of the data to be presented in later sections. They are discussed in detail below.

a. Selection of cases

A total of 37 cases that occurred between November and March of 1993, 1994, and 1995 were analyzed for this study. Cases were selected to provide a variety of synoptic weather scenarios, based upon inspection of the 0000 (all times UTC) surface analysis from NCEP and plots of icing PIREPs for the 6-h window centered on 0000. Essentially all surface features of winter weather systems, synoptic-scale forcing mechanisms from the surface to 500 mb, surface airmass origins, and surface precipitation types were examined. A summary of most of the weather features, forcing mechanisms, surface airmass origins, and precipitation types associated with the 37 cases is given in Table 1.

b. Definitions of surface features

A rigorous set of guidelines was created to allow for consistent labeling of features on both surface and upper air (850, 700, and 500 mb) charts. Six airmass categories were developed, based upon the possible origins of surface air masses over the continental United States (see Table 2a); arctic (A), continental (C), East Coast (E), gulf (G), Pacific (P), and West Coast (W). Origin of the air mass was determined using streamlines of wind reports from NCEP surface maps. To further define air masses, surface temperature and moisture guidelines were established, as well as geographical constraints. ''Continental'' was used as a catchall category for air masses that have lost their original, distinctive characteristics (e.g., an arctic air mass that has been modified by heating over several days), as well as those that met the specific definition for this air mass.

A total of 35 sector categories were developed to define different portions of synoptic-scale cyclones, anticyclones, and the fronts and troughs associated with them (see Table 2b). Figure 1 graphically depicts the sectors of an idealized synoptic-scale cyclone and its attendant large-scale air masses. Sectors numbered 1–25 are associated with *active* fronts (those which are in motion), surface lows, troughs, and large-scale areas far away from these features. Additional numbers (41, 45–48, 52–54, 56, and 57) have been assigned to sectors along or near *stationary* fronts that had signatures similar to the active frontal sectors described above. For example, a ''12'' is assigned to the sector just behind (on the cold side of) an active arctic front and a ''52'' (12 + 40, all stationary features have numbers 40 larger than their corresponding active features) is assigned to the sector just on the cold side of a stationary front with arctic frontal characteristics (e.g., strong cold advection on the cold side of the front, source air from Canada, and/or polar regions). Since weather phenomena can vary greatly depending upon the nature of frontal motion, stationary and active frontal sectors have been defined separately to assess their relative importance for aircraft icing.

The highly specific breakdown of weather systems into sectors allows for the identification of such locations as ''in the vicinity of a Pacific cold front,'' for example, as likely to contain icing conditions. Furthermore, the breakdown of individual frontal regions into prefrontal, on the front, and postfrontal sectors allows for the assessment of *which portion* of a particular frontal type is most likely to contain this hazard.

c. Surface precipitation and cloud analysis

To assess the relationship between PIREPs of icing and surface precipitation type or amount of cloud cover present, a gridded analysis of the 0000 surface airways observations (SAOs) was performed. A latitude–longitude (lat–long) grid of 0.25° lat × 0.25° long boxes was created over the United States. The precipitation or greatest cloud coverage (when precipitation was not occurring) reported by the SAO closest to the centroid of each grid box was assigned to that box. Six categories were used for precipitation: snow, rain, drizzle, freezing

TABLE 1. Summary of 37 cases used in the study. Boxes are marked with an "X" if the synoptic weather feature indicated for each column was observed. Values at the bottom are the total number of cases that had the weather feature identified at the top of each column.

Date	Arctic front	Occluded front	Pacific front	Warm front	Surface trough	Dryline	Deep low (<1000 MB)	Stationary front	Closed low aloft	Overrunning	Freezing precipitation	Snow	Rain	Drizzle	Thunder	Arctic air mass	Continental air mass	West Coast air mass	Pacific air mass	Gulf air mass	East Coast air mass
10 Jan 93	X				X			X	X	X	X	X	X	X		X	X	X	X		X
19 Jan 93	X	X	X	X	X			X	X	X	X	X	X	X	X	X	X	X	X	X	X
20 Jan 93	X	X	X	X	X			X		X	X	X	X	X	X	X	X	X	X	X	X
12 Feb 93	X	X		X	X			X	X	X	X	X	X	X	X	X	X	X	X	X	X
21 Feb 93	X		X	X	X		X	X	X	X	X	X	X	X		X	X	X	X	X	X
26 Jan 94	X	X	X	X		X		X	X	X	X	X	X	X	X	X	X	X	X	X	X
28 Jan 94	X		X	X	X			X	X	X	X	X	X	X	X	X	X			X	X
30 Jan 94	X				X			X				X	X	X		X	X	X		X	X
1 Feb 94	X			X	X			X				X				X	X	X			
8 Feb 94	X	X	X	X	X	X	X	X	X	X		X	X	X		X	X	X	X	X	X
11 Feb 94	X		X	X	X			X	X	X	X	X	X	X	X	X	X	X	X	X	X
14 Feb 94	X		X	X	X				X			X	X			X	X	X	X	X	
17 Feb 94	X		X	X			X	X	X				X	X		X	X	X		X	X
19 Feb 94	X	X	X	X	X	X	X	X	X			X	X		X	X	X	X	X	X	X
22 Feb 94	X		X		X	X		X	X		X	X	X	X	X	X	X	X	X	X	X
23 Feb 94	X		X	X	X	X		X	X	X	X	X	X	X	X	X	X	X	X	X	X
25 Feb 94	X		X	X	X	X	X	X	X	X	X	X	X	X		X	X	X	X	X	
1 Mar 94			X	X	X				X		X	X	X	X	X	X	X	X	X	X	X
3 Mar 94	X		X	X	X		X		X	X	X	X	X	X	X	X	X	X	X	X	X
4 Mar 94	X		X	X	X		X		X	X	X	X	X	X		X	X	X	X		X
8 Mar 94	X	X	X	X	X	X		X	X		X	X	X	X	X	X	X	X	X	X	X
10 Mar 94	X		X	X	X			X	X	X	X	X	X	X	X	X	X	X		X	X
16 Mar 94	X		X				X	X				X	X	X	X	X	X	X		X	X
20 Mar 94		X	X	X	X		X					X	X			X	X	X	X	X	
24 Mar 94	X		X	X	X	X	X	X	X	X	X	X	X	X	X	X	X	X		X	X
1 Nov 94			X	X	X			X	X				X	X	X		X	X	X	X	X
14 Nov 94	X		X	X			X	X				X	X	X		X	X	X	X	X	X
6 Jan 95	X	X		X	X		X		X	X	X	X	X	X		X	X	X	X		X
7 Jan 95	X		X	X	X			X		X	X	X	X	X	X	X	X	X	X	X	X
12 Jan 95	X			X	X	X	X	X		X	X	X	X	X		X	X	X	X	X	X
17 Jan 95	X		X	X	X		X	X	X	X	X	X	X	X		X	X	X	X	X	X
15 Feb 95			X	X	X		X		X	X	X	X	X	X		X	X	X	X	X	X
28 Feb 95	X			X	X			X		X	X	X	X	X	X	X	X	X		X	X
5 Mar 95	X			X	X	X		X	X	X	X	X	X	X		X	X	X		X	X
7 Mar 95	X		X	X	X			X		X	X	X	X	X	X	X	X	X	X	X	X
8 Mar 95	X			X	X			X	X	X	X	X	X	X	X	X	X	X			X
21 Mar 95		X	X	X	X		X		X			X	X	X	X		X	X	X	X	X
	3	1	2	3	3	1	1	2	2	2	2	3	3	3	2	3	3	3	2	3	3
Total cases: 37	2	0	8	3	3	0	6	9	7	4	6	5	6	3	1	5	7	6	7	2	3

rain, freezing drizzle, and ice pellets. Fog and thunder occurrences were also matched to each box. Five categories were used for cloud cover, and the following hierarchy was used for the cloud cover assigned to each box, regardless of altitude: obscured, overcast, broken, scattered, and clear. More than one precipitation type (if the nearest SAO reported several types, e.g., snow mixed with rain), but only one cloud cover, could be assigned to each box. This allowed for the calculation of the areal extent of each precipitation type and cloud coverage. A maximum search radius of 75 km was used to ensure that the data from any one SAO could not be extrapolated to a grid point more than 75 km away. This was especially important in states such as Nevada, where SAO coverage is sparse. Gaps can still exist in the coverage of SAO data using this method.

d. Pilot reports of icing

Voice PIREPs of icing severity and type were compared to the locations of air masses, sectors, precipitation types, and cloud coverages. To provide an adequate number of observations, PIREPs for the 6-h window centered on 0000 were used for each case. Although most surface weather features were in motion during the time window, analyses for 0000 are considered to

TABLE 2a. Definitions of (a) surface airmass types, (b) cyclone sectors, and (c) synoptic-scale forcing mechanisms.

(a) Surface airmass definitions

Air mass	Origin	Temp ranges	Typical winds	Limits to area	Other characteristics
A = Arctic	Polar/Canadian	$<10°C$	Northerly component	None	None
C = Continental	Continental	All	Any	None	Usually been over continental United States for a few days—modified; other air masses that have been significantly modified
E = East Coast	Atlantic	All	Easterly component	Usually east of Appalachians	None
G = Gulf	Gulf of Mexico	$>10°C$	Southerly component	East of the Rocky Mountains	None
P = Pacific	Pacific	All	Westerly component	West of the Continental Divide	Dewpoint depression $<10°C$
W = West Coast	Pacific	All	Westerly component	West of the first major mountain ranges	None

be representative. Brown et al. (1997) showed that the use of a 6-h versus a 3-h time window for PIREP comparison with icing algorithm output changed statistical results by only 5%. Though different data were compared to icing PIREPs in that study, the results imply that the larger time window should not have much effect on the results of this paper.

Icing severity is defined by the accumulation rate of the ice and the hazard it presents to the aircraft, while type is determined by the appearance of the ice as it has frozen onto the airframe (see Table 3; Air Weather Service 1980). Specific combinations of icing severity and type are used in later sections, including categories for any icing that pilots report (of trace or greater severity and any type, hereafter referred to as ''general'') and for some of the worst icing that pilots report (of moderate or greater severity and clear or mixed type, hereafter referred to as ''worst''). The worst category was created based on results that show that clear and mixed icing, which can be formed via aircraft encounters with large supercooled liquid water droplets and/or regions of high liquid water contents at high temperatures ($>-12°C$), caused the greatest decrease in aircraft performance and can continue to do so, even after attempts to deice the aircraft have been made (Ranaudo et al. 1984; Shin et al. 1991; Politovich 1996). Although pilot reports of moderate icing of any type are meant to indicate significant performance degredation, moderate or greater intensity rime icing is not included in this category because rime icing is typically formed by the freezing of small droplets onto an airframe at colder temperatures, usually causes a smaller performance degradation and is more easily removed (Ranaudo et al. 1984). It is important to note that the worst category is not intended to imply that a pilot report of ''moderate clear icing'' is an indication of a greater perfomance degredation than a ''severe rime icing'' report. Since large drop icing is an area of great concern to the aviation community, the worst PIREP category is limited to those PIREPs that tend to be reported in large drop conditions.

Brown et al. (1997) addressed several caveats of the use of PIREPs as a verification database. Outside of research aircraft documentation of winter storms, however, PIREPs are the only data source of the existence of icing aloft. For this study, more than 2700 PIREPs have been used to create a large volume of observations. Although the data from a few PIREPs can be questioned, general trends based upon thousands of PIREPs are probably well founded. PIREPs used in this study were for altitudes below 3 km ($\sim$10 000 ft) AGL (above ground level), since they are most likely to relate to surface phenomena. Overall, $\sim$75% of general and $\sim$80% of worst PIREPs occurred below 3 km AGL.

e. Data normalization

For each case studied, polygons that enclosed the surface locations of each airmass and cyclone sector were drawn. The widths of cyclone sector polygons were approximately 100 km along surface fronts and 200 km immediately ahead of and behind surface fronts, in all cases. These values were chosen to allow for movement of fronts during the 6-h PIREP time window. Each polygon was then overlaid with a silhouette of the United States, and the areal extent of the intersection was calculated in square kilometers. The sum of the areal extents of each silhouetted airmass and cyclone sector polygon, as well as precipitation type/cloud cover grid box, was calculated for all cases (Fig. 2). Examples of polygons and a precipitation grid will be presented in section 3.

The lat–long of each individual PIREP was digitally matched to an airmass and a sector polygon. These matches were tallied over all 37 cases and placed into bins according to the reported icing severity and type. Raw counts can be misleading, however, as many more PIREPs could have occurred within a certain air mass or sector simply because it had a large areal extent and/

TABLE 2b. Sector definitions

Sector	Ahead/on/behind what feature	Other
1	50–250 km ahead of Pacific or continental front	
2	>50 km behind dryline	
3	50 km either side of dryline	
4	>250 km behind warm front	Flow typically toward warm front, usually gulf air
5	50–250 km behind warm front	
6	50 km either side of warm front	
7	50–250 km ahead of warm front	
8	250–650 km ahead of warm front	Significant cross-frontal wind component, does not reach center of arctic high
9	Well within East Coast air mass	Away from fronts, troughs, low centers
10	Around occluded low	Size of area is proportional to strength of low
11	Well within arctic air mass	Away from fronts, troughs, low centers
12	50–250 km behind Canadian or arctic front	
13	50 km either side of Canadian or arctic front	
14	50–250 km ahead of Canadian or arctic front	
15	Well within Pacific or West Coast air mass	Away from fronts, troughs, low centers
16	50–250 km behind Pacific or continental front	
17	50 km either side of Pacific or continental front	
18	Around main surface low	Size of area is proportional to strength of low
19	50–250 km behind surface trough	
20	50 km either side of surface trough	
21	50–250 km ahead of surface trough	
22	50–250 km behind occluded front	
23	50 km either side of occluded front	
24	50–250 km ahead of occluded front	
25	Center of continental air mass	Away from fronts, troughs, low centers
41	50–250 km ahead of stationary Pacific or continental front	Similar to sector 1
45	50–250 km behind stationary warm front	Similar to sector 5
46	50 km either side of stationary warm front	Similar to sector 6
47	50–250 km ahead of stationary warm front	Similar to sector 7
48	250–650 km ahead of stationary warm front	Similar to sector 8
52	50–250 km behind stationary arctic front	Similar to sector 12
53	50 km either side of stationary arctic front	Similar to sector 13
54	50–250 km ahead of stationary arctic front	Similar to sector 14
56	50–250 km behind stationary Pacific or continental front	Similar to sector 16
57	50 km either side of stationary Pacific or contiental front	Similar to sector 17

TABLE 2c. Forcing mechanisms

Feature	Mechanism
Surface cold front	Active surface cold front within ~300 km
Surface warm front	Active surface warm front within ~300 km
Surface stationary front	Stationary front within ~300 km
Surface low	Surface low within ~300 km
Surface trough	Surface trough within ~300 km
Terrain	Terrain forcing (upslope) evident at location
Lake effect	Lake-effect dynamics evident at location
Upper trough	Upper trough within ~300 km
Upper low	Upper-level closed low within ~300 km
Overrunning	Within or beneath overrunning conditions
Cold advection	Within, above, or below significant cold advection
Warm advection	Within, above, or below significant warm advection
None	No forcing mechanism evident at location

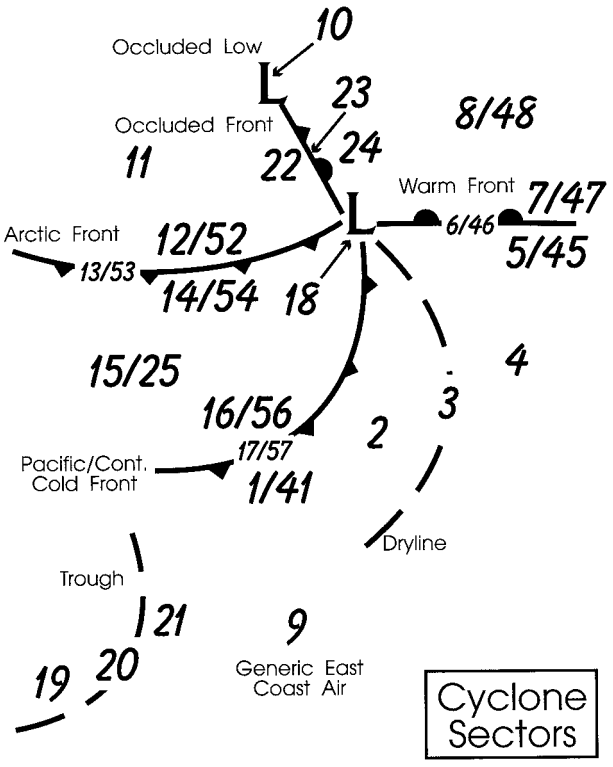

FIG. 1. Locations of cyclone quadrants for an idealized surface weather system. Locations of the surface warm, occluded, arctic cold, and Pacific/continental cold fronts, dryline, surface trough, and main low and occluded low pressure centers are indicated using standard symbols. When two numbers are given at a location, the first and second numbers are for the active and stationary fronts of this type.

TABLE 3. Definitions of icing severities (intensities) and types used in PIREPs of icing. From Air Weather Service (1980).

Category	Pilot reporting definition
Icing severity*	
Trace	Ice becomes perceptible. Rate of accumulation is slightly greater than rate of sublimation. It is not hazardous even though deicing/anti-icing equipment is not utilized, unless encountered for an extended period of time (over 1 h).
Light	The rate of accretion may create a problem if flight is prolonged in the environment (over 1 h). Occasional use of deicing/anti-icing equipment removes/prevents accretion. It does not present a problem if the deicing/anti-icing equipment is used.
Moderate	The rate of accretion is such that short encounters become potentially hazardous and use of deicing/anti-icing equipment, or diversion, is necessary.
Severe	The rate of accretion is such that deicing/anti-icing equipment fails to reduce or control the hazard. Immediate diversion is necessary.
Icing type	
Rime	Rough, milky, opaque ice formed by the instantaneous freezing of small supercooled droplets as they strike the aircraft. The fact that the droplets maintain their nearly spherical shape upon freezing and thus trap air between them gives the ice its opaque appearance and makes it porous and brittle.
Clear	Glossy, clear, or translucent ice formed by the relatively slow freezing of large supercooled droplets. The large droplets spread out over the airfoil before complete freezing, forming a sheet of clear ice.
Mixed	A mixture of rime and clear ice.

* Numerical equivalents: 1 = trace, 2 = trace/light, 3 = light, 4 = light/moderate, 5 = moderate, 6 = moderate/severe, and 7 and 8 = severe.

or occurred on many days. To account for this, the total number of PIREPs matched to each air mass and sector has been divided by the total areal extent of that air mass or sector. This normalized result, which will hereafter be referred to as the *threat*, is the number of PIREPs per 10^6 km^2. Thus, small areas associated with a large number of PIREPs were given proper credit for the greater icing hazard they presented to aircraft. Threat values are simply the density of icing PIREPs and should not be confused with an absolute ''risk'' or ''chance'' of encountering icing in a particular portion of a winter weather system.

The matching of PIREPs to SAOs was done much like the gridding of SAOs for the calculation of areal extent of each precipitation type. Using the lat–long pair of each PIREP and the lat–long pairs of all SAO sites, each PIREP was matched to the SAO stations closest to it. Since the location of a PIREP may not be exact and surface precipitation type can vary greatly over short distances and small changes in time, the PIREP was matched to all SAOs within 75 km. Thus, all precipitation types, fog, thunder, and the greatest amount of cloud cover reported by these SAOs at 0000 were matched to the PIREP.

This method was chosen rather than matching the PIREP to the single nearest SAO to account for the variety of observation platforms used in SAOs, including automated weather stations. AWOS (Automated Weather Observing System) and AMOS (Automated Meteorological Observing System) stations do not report the occurrence of precipitation or type, except when augmented by observer comments. ASOS (Automated Surface Observing System) stations can have difficulty distinguishing precipitation types, especially for mixed precipitation and between rain, drizzle, freezing rain, and freezing drizzle (Ramsay 1996). Also, the use of ceilometers at these stations limited the usefulness of cloud cover information, as they only provided data up to 12 000 feet (~3.65 km) AGL. Augmented precipitation data from these stations were used whenever possible to help alleviate these problems. Of SAOs used in this study, 82.0% were recorded by human observers, 14.1% by AWOS stations, 3.9% by ASOS stations, and 1.5% by AMOS stations. Only 28.1% of the PIREPs used in this study were matched to only one surface station. Many PIREPs were likely to have been matched to an automated SAO site, but rarely (~5% of the time) did these stations provide the only precipitation and cloud cover data for a particular PIREP.

f. Icing ''events'' and comparison with other observational data

Recent studies of the nature of PIREPs have shown that they are not uniform in their geographic distribution, but occur more frequently in high traffic volume areas, such as the east coast, Great Lakes and west coast regions of the United States (Politovich and Olson 1991; Schultz and Politovich 1992; Brown et al 1993). For this reason, statistics associated with weather phenomena that often occur in high traffic regions could be artificially high. As an alternative to results based on summed values from individual PIREPs, when two or more PIREPs with moderate or greater icing severity occurred close to each other in location and altitude, they were grouped into an icing ''event.'' Using this method, two PIREPs of moderate or greater severity that occurred over rural Montana were given the same credit as a group of 20 PIREPs that occurred over the busy Chicago airspace. Both events were assumed to be indicative of one occurrence of icing conditions in their respective areas. Events were also determined by the location of groups of PIREPs relative to major synoptic features. PIREPs from all altitudes were included into icing events, since they are matched to weather features from the surface to 500 mb. Forbes et al. (1993) used similar methods to identify icing events.

Each event was matched to an air mass and a sector. The altitudes of the PIREPs within the event were examined to determine at what level it occurred. Us-

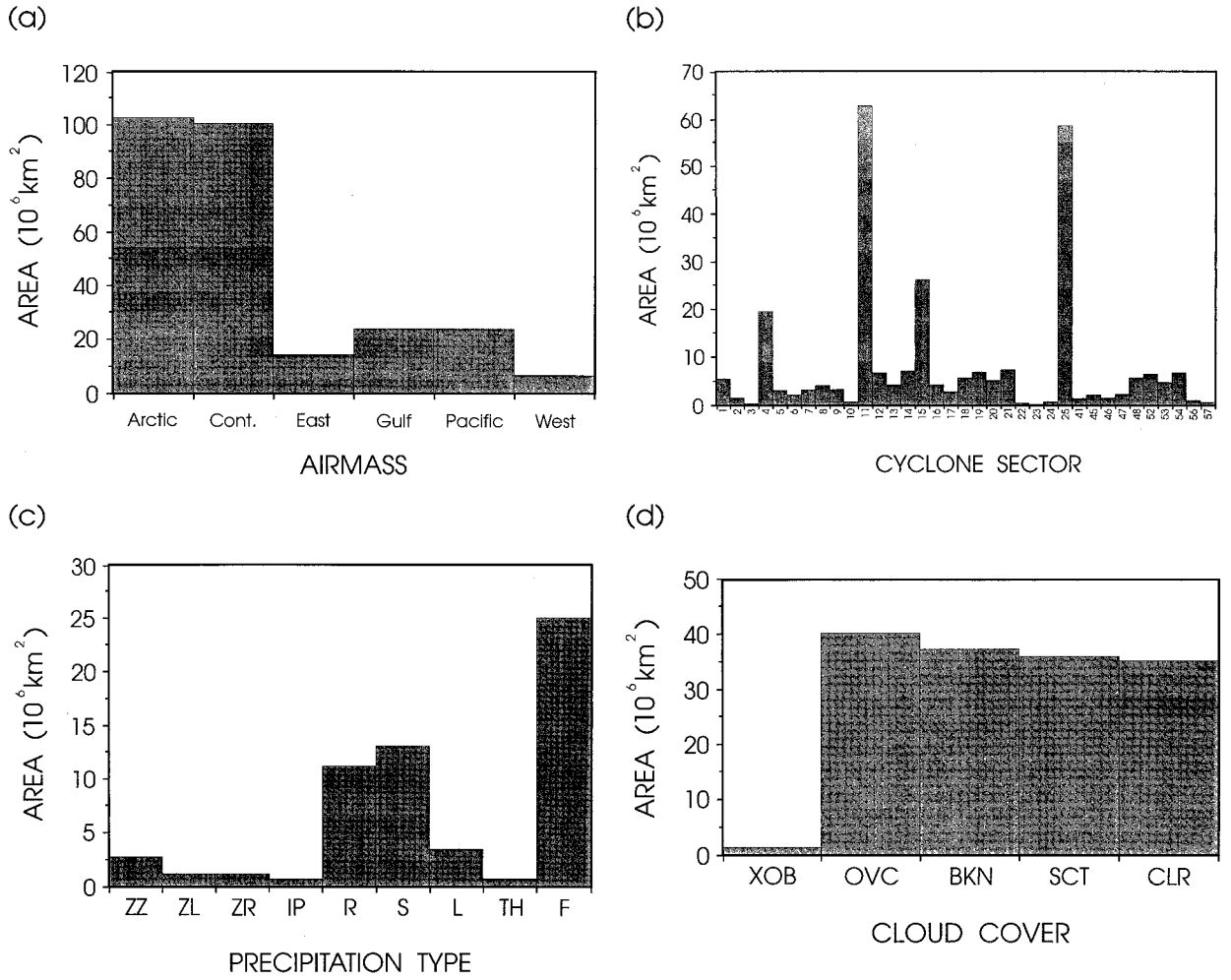

FIG. 2. Total areal extent (10^6 km^2) for all 37 cases by (a) airmass type, (b) cyclone sector, (c) precipitation type, and (d) cloud cover. Airmasses and cyclone sectors are defined in Table 2. Precipitation types are ZL = freezing drizzle, ZR = freezing rain, IP = ice pellets, R = rain, S = snow, L = drizzle, TH = thunder, F = fog, and ZZ = all freezing precipitation types combined (ZL, ZR, and IP). Cloud coverages are XOB = obscured, OVC = overcast, BKN = broken, SCT = scattered, and CLR = clear.

ing the analyzed surface and upper-air charts, two primary synoptic forcing mechanisms that appeared to be related to the icing event were assigned to it. The dominant surface precipitation types that occurred directly beneath the event were also assigned to it. Finally, hard copy maps of the NWS national radar mosaic, visible satellite imagery, the lightning detection network composite (Newhouse 1991), and SAOs were visually inspected to assign a simple yes/no to each event for the occurrence of 1) at least video integrated processor (VIP) level 1 reflectivity ($\geq$18 dBZ$_e$), 2) visible cloud, and 3) lightning or thunder within the polygon of lat–long points outlining the icing event. NWS snow cover maps and SAO reports of cloud cover were inspected to avoid mislabeling cloud-free areas.

Radar reflectivity and lightning/thunder matches were used to determine the frequency of occurrence of these phenomena in association with icing events. The cloud cover field was used as a measure of the validity of the PIREP dataset. If a PIREP occurred where clouds were not present, the location of the PIREP was likely misreported. ''Stray'' PIREPs with trace or light severity that occurred far from all other PIREPs were also tested against cloud cover, since these PIREPs were most likely to contain gross reporting errors. Though icing events take into account discrepancies in air traffic and provide additional information on the occurrence of icing with the weather phenomena outlined above, they are subjective in nature. Icing events could only be roughly matched to air masses, cyclone sectors, precipitation, and cloud cover, since no single lat–long pair could be assigned to them. For these reasons, icing events are presented in an effort to support the results found using individual PIREPs of icing. Results from icing events will be discussed in section 4f.

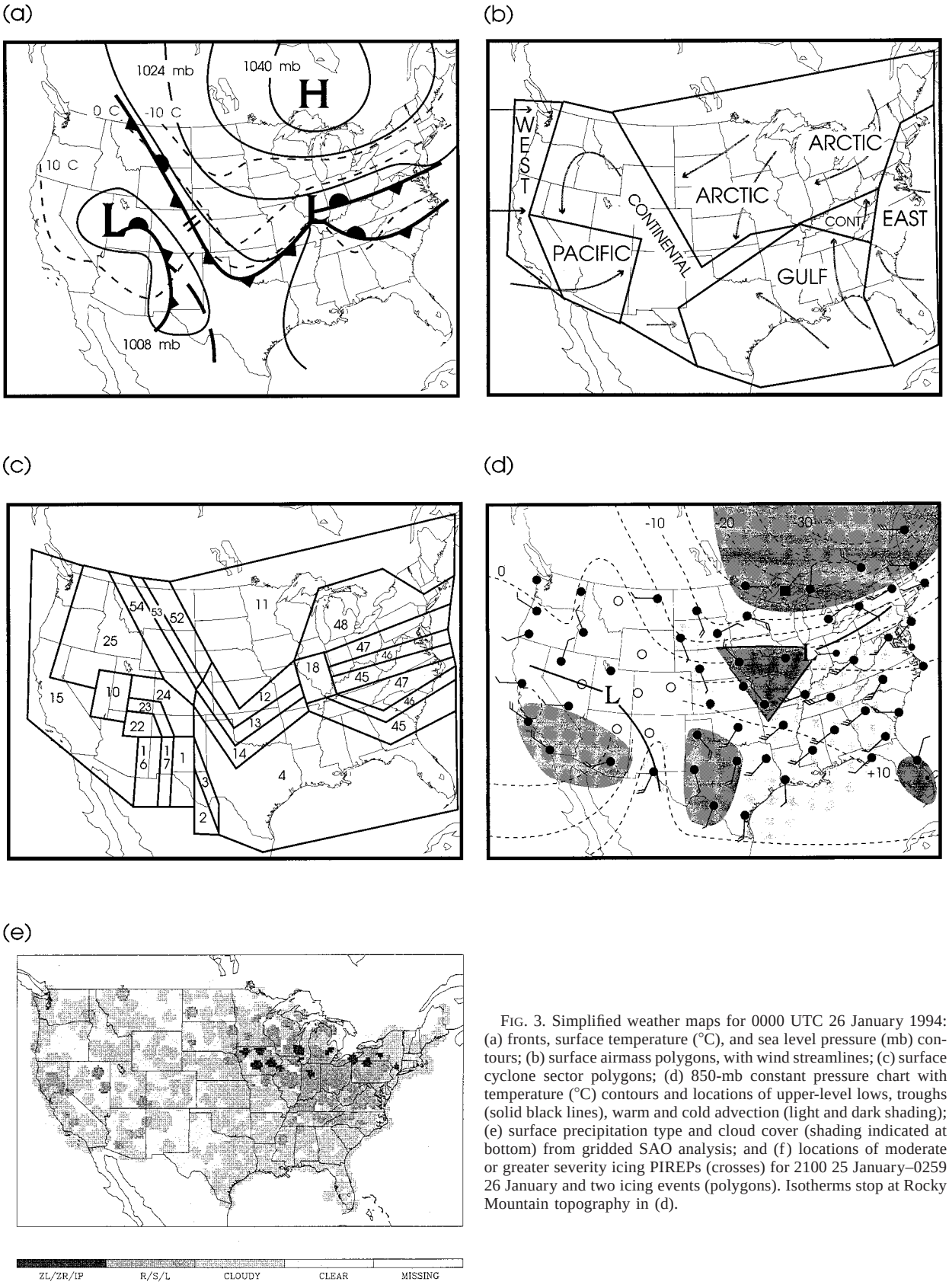

FIG. 3. Simplified weather maps for 0000 UTC 26 January 1994: (a) fronts, surface temperature (°C), and sea level pressure (mb) contours; (b) surface airmass polygons, with wind streamlines; (c) surface cyclone sector polygons; (d) 850-mb constant pressure chart with temperature (°C) contours and locations of upper-level lows, troughs (solid black lines), warm and cold advection (light and dark shading); (e) surface precipitation type and cloud cover (shading indicated at bottom) from gridded SAO analysis; and (f) locations of moderate or greater severity icing PIREPs (crosses) for 2100 25 January–0259 26 January and two icing events (polygons). Isotherms stop at Rocky Mountain topography in (d).

(f)

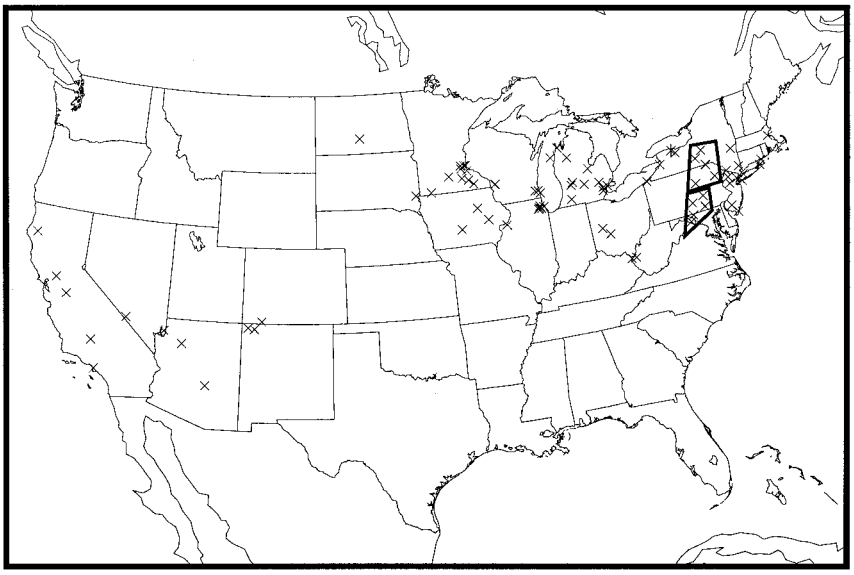

FIG. 3. *(Continued)*

3. An example case: 26 January 1994

Simplified maps from an example case (26 January 1994, hereafter referred to as 26JAN) are discussed to give a better understanding of the methods described above. This case was one of the most complicated encountered in this study and included nearly every class of surface feature, precipitation type, and forcing mechanism. A total of 205 PIREPs of trace or greater icing severity were recorded in 6 h surrounding 0000 26JAN. Specific surface and upper-air features of interest in this study are highlighted with italics.

a. Surface weather analysis

At 0000 26JAN, a strong high pressure system was centered over Ontario, Canada (Fig. 3a). The *arctic* air mass (see Fig. 3b) associated with this high brought temperatures below −10°C to the northern Great Plains, and as low at +10°C to central Oklahoma. The southernmost extent of the arctic air mass had been modified to reach temperatures in excess of +10°C, which made it *continental* in type (see Table 2a). The arctic air mass was bordered on its southwestern edge by a stationary front, which extended from the Montana–Canada border to eastern Colorado. This *stationary arctic front* (sector 53 in Fig. 3c) was the remains of an arctic cold front that became dammed against the eastern slope of the Rocky Mountains. The southern extent of this front remained active (an *active arctic front*) and existed in a bow shape from southeast Colorado to the Oklahoma–Texas border, then northeastward to connect with a weak low pressure center near St. Louis, Missouri. Two stationary fronts extended from this low to the Delaware and North Carolina coasts. Both fronts were associated with strong warm advection at 850 mb (Fig. 3d) and 700 mb, and were labeled *stationary warm fronts.*

To the south of the stationary fronts, winds were from the east and southeast from Virginia to Florida, making this an *East Coast* air mass. From western Georgia to central Texas, winds were from the south, bringing air from the Gulf of Mexico, making this a *gulf* air mass. Between the two fronts and west of the Appalachian mountains, winds were southerly, but the air did not have a clear origin. The air mass was labeled continental, since its characteristics were markedly different from the gulf air mass to the south and the stable East Coast air mass, which was not able to cross the mountain chain.

An *occluded low* pressure center was located in southwestern Utah, with an *occluded front* bowing southeastward to New Mexico. The front continued southward into Mexico as a *Pacific cold front*, as the air behind it had a strong westerly component, with a fetch over the Pacific Ocean. A *Pacific* air mass was in place behind this front. A *dryline* trough extended from the southern end of the occlusion to southwestern Texas. Dry air from Mexico was behind this trough, making that airmass continental in type. Continental air also existed to the north of the occluded front, as this air had a general downslope component from the Continental Divide region. Finally, moist air was arriving onshore from Washington to California, from the coastline eastward to the first major mountain ranges, characterizing this narrow strip of air as a *West Coast* air mass.

Surface precipitation type varied greatly across the

United States on 26JAN, as seen in Fig. 3e. A large swath of rain, drizzle, and fog was reported from Pennsylvania to Kansas, while spotty rain occurred along portions of the West Coast. Snow was reported along the Canadian border and in parts of the southwest United States, while freezing drizzle, freezing rain, and ice pellets fell in a thin line from Iowa to New York. The majority of the eastern United States was blanketed beneath obscured and overcast skies, while patches of thick cloud covered the western United States.

b. Upper-air chart analysis

A brief examination of the 850-mb chart (Fig. 3d) gives an indication of the major synoptic-scale forcing mechanisms at work aloft on 26JAN. A weak upper low was centered over northwest Indiana, with an area of *warm advection* to its south and east. The strongest warm advection was in place from Pennsylvania southward to North Carolina, immediately above the two surface stationary warm fronts mentioned earlier. The vertical structure in this region showed strong temperature increases with height, indicative of *overrunning*. Strong *cold advection* was occurring along the U.S.–Canada border from the Great Lakes to Maine. An *upper-level closed low* was also centered above the surface occluded low in Utah. Cold advection was evident to the south of this low, behind the surface Pacific cold front. Several *upper-level troughs* extended from the two upper lows, and most were indicative of the upward continuation of surface fronts, though some were merely wind shift lines.

c. Icing PIREP and event analysis

A plot of the 93 icing PIREPs with moderate or greater severity recorded for the 6-h window centered on 0000 26JAN is shown in Fig. 3f. On this day, most PIREPs occurred 100–400 km to the north of the northern stationary warm front and to the northwest of the weak surface low centered in Illinois. Those PIREPs between Chicago and Boston were within cyclone sectors 47 and 48, and those in Iowa, Minnesota, and North Dakota were within sector 11 (Fig. 3c). The PIREPs in these regions were all within the arctic air mass.

PIREPs were placed into a total of 18 distinct icing events for this case, based upon groupings of the reports with similar altitude ranges and locations relative to weather features. Two events highlighted in Fig. 3f were close together in location, but different in many ways. The southern event occurred between 2 and 5.5 km above mean sea level (MSL), was just north of the northern stationary front, and contained mostly rime icing. The northern event occurred between 1 and 2 km MSL, was much farther north of the front, and contained mostly mixed icing. Both events were associated with overrunning and warm advection, but the northern event occurred within a 2-km-deep layer of freezing drizzle beneath the upper-level trough, while the southern event occurred well above the upper trough and the melting layer that accompanied it. The two events also occurred above different surface precipitation types (north: ZL/IP, south: R), and only the southern event had reflectivity $\geq$18 dBZ_e within it.

4. Results

Using the methods described above, data from PIREPs and icing events were accumulated for all 37 cases. Overall statistics were calculated to indicate preferred locations for icing. The statistics presented here will concentrate on two ranges of icing reports; all icing intensities and types (general), and icing of moderate or greater severity combined with clear or mixed in type (worst). The first category is used to indicate the occurrence of *any icing*, while the second indicates some of the *worst icing* encounters made by pilots. Results based upon individual PIREPs will be discussed in sections 4a–e, while those for *icing events* will be discussed in section 4f. When comparing PIREPs and icing events to surface weather features, the PIREPs are considered to be ''within'' a certain surface air mass, sector, etc., rather than above it. The purpose of this section is to identify such features by simple examination of surface and upper-air charts and model output. Airmass type can change with altitude, as in an overrunning situation (where gulf air may exist above arctic air). Changes in airmass type with altitude are typically handled by the identification of forcing mechanisms aloft such as upper troughs and overrunning. Descriptions of the meteorology relating to the air masses, cyclone sectors, precipitation types, and the aircraft icing associated with them are based upon the cases studied here, unless otherwise specified.

a. Air masses

The distribution of PIREPs with airmass type for all altitudes is shown in Fig. 4a. Most of the 2702 general PIREPs occurred within arctic air masses, while the remaining reports were relatively evenly distributed among the other air masses. Similar results were found for the 278 worst PIREPs. In both cases, gulf air masses contained the fewest icing reports, while the remaining air masses contained $\sim$10% of the PIREPs in either category. Considering the relative size of arctic air masses (see Fig. 2a), their cold nature, and the fact that they often covered regions with high air traffic (e.g., the Great Lakes region), this result was not surprising. Simple counts and percentages of PIREPs can be extremely misleading, however. Although many PIREPs occurred within the arctic air masses, these air masses covered the largest amount of summed area (1.02×10^8 km^2) for all cases, while some other air masses covered a relatively small amount of area (e.g., East = 1.60×10^7 km^2).

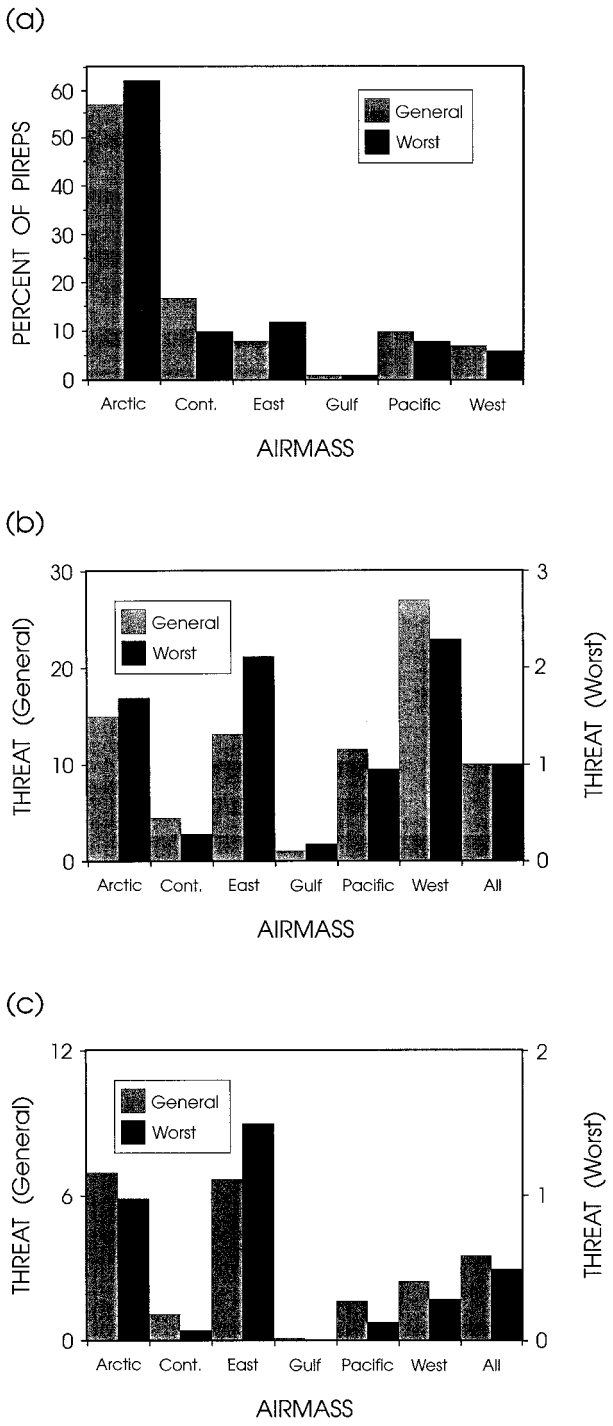

FIG. 4. (a) Percentages and (b) threats (counts/areal extents, PIREPs/10^6 km^2) of general (gray columns) and worst (black columns) PIREPs for all altitudes matched to air masses. (c) Threats of general and worst PIREPs for altitudes $\leq$1 km AGL.

Airmass icing *threats*, which represent the number of PIREPs encountered within these air masses per unit area, give a better indication of the likelihood that pilots would encounter icing conditions within them. Threats were calculated to show the likelihood that icing will occur within any given portion of the United States (all category), for comparison with individual airmass types. For general icing, only the threat for the West Coast air masses far exceeded that for all locations, while threats for the East Coast and arctic air masses were slightly higher (see Fig. 4b). The gulf and continental air masses were relatively free of icing PIREPs. Results were similar for worst icing, but the West Coast, East Coast, and arctic air masses all had notably higher threats than for all locations.

When general and worst PIREPs were limited to only those which occurred at or below 1 km (3280 ft) AGL, the East Coast and arctic air masses had threats that far exceeded that of the West Coast (Fig. 4c). This is likely attributable to the relatively deep nature of the moisture associated with weather systems as they impacted the West Coast. Since these storms were coming off of the ocean, the low-level temperatures within the systems were typically above freezing, and surface precipitation was in the form of rain or drizzle. The combination of these factors often limited occurrences of icing conditions at low levels, depending upon the temperature (T) profiles of individual weather systems.

In contrast, the Arctic systems tended to be shallow ($<$3 km deep) and cold in nature. Recent results from studies performed in northeast Colorado have shown that clouds containing liquid water within arctic air masses tended to occur at $T \geq -12$°C, while clouds often contained significant amounts of ice crystals when they were colder than about -15°C (Politovich and Bernstein 1995; Rasmussen et al. 1995). Such results may not be applicable to arctic air masses, in general, however. Many of the East Coast air masses were associated with cold, easterly flow around high pressure systems centered in the northeastern United States and southeastern Canada. In those cases, cold, stably stratified air traversed the Atlantic Ocean, brought relatively shallow moisture inland, and often dammed it against the east slope of the Appalachians.

b. Cyclone sectors

The reader should refer to Fig. 5a as a guideline for the discussion that follows. Again, a relative threat for a particular region can be gained via comparison with the threat calculated for all sectors combined.

Figure 5b depicts the distribution of general PIREPs with cyclone sector. There was a tendency for the most icing to occur in the largest sectors (Fig. 2b). This was especially true deep within arctic (sector 11), but not so for gulf air masses (sector 4). Sector 11 made up the majority of the arctic air masses, which had the highest percentage statistics for PIREP occurrences, while sector 4 made up the majority of the gulf air masses, which had the lowest PIREP percentages. Two relatively small sectors captured a fairly large percentage of the PIREPs: 250–600 km ahead of active and stationary warm fronts

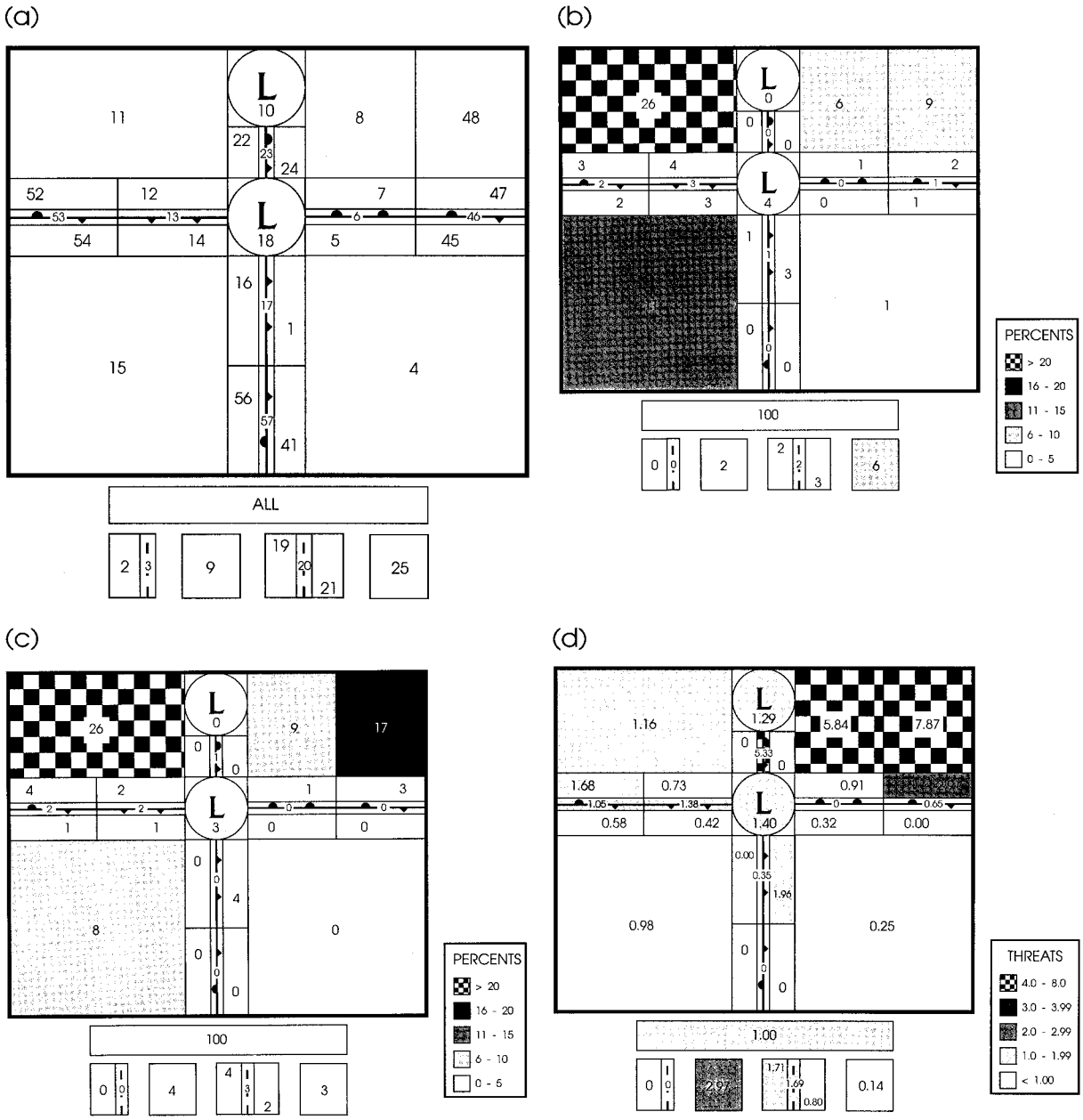

FIG. 5. (a) Sector number key. (b) Percentages of general and (c) worst PIREPs matched to cyclone sectors. (d) Threats (counts/areal extents, PIREPs/10^6 km^2) for worst PIREPs matched to cyclone sectors. Sector numbers in key are defined in Table 2b. Values of percentage and threat are indicated within the sectors. Fill patterns for percentage and threat ranges are indicated in the lower-right corners of (b)–(d). Locations and types of fronts and troughs are indicated.

(sectors 8 and 48). All other small sectors captured $<5\%$ of the PIREPs. Trends were similar for worst PIREPs (Fig. 5c), but combined percentages for the highly similar sectors 8 and 48 (26%) equaled the value for deep within arctic air masses (sector 11), while their combined total area was less than one-sixth that of sector 11.

Charts of the threat of icing by sector provide a strong indication of what portions of synoptic-scale weather systems contained the most icing, per unit area. Threats of worst icing are shown in Fig. 5d. Trends in values calculated for general icing (not shown) were very similar. As expected from the percentages and areal coverages discussed above, the sectors 250–600 km ahead (on the cold side) of active and stationary warm fronts (8 and 48) had the highest threats. Worst icing was ~6–8 times more likely to occur there than for a randomly selected portion of a surface weather map (''all'' category).

These results make intuitive sense, since the area to

the north of these surface fronts was often the location of relatively high (warm) cloud-top temperatures, low surface temperatures (often below freezing in winter), high moisture content, and widespread light precipitation that was sometimes freezing in nature. Such features were indicative of a deep layer of saturated conditions with temperatures below freezing, where icing conditions are expected. Warm cloud tops and light precipitation suggest a lack of efficient ice formation in the cloud layer, which would scavenge out supercooled liquid water via riming (Politovich and Bernstein 1995; Rutledge and Hobbs 1983). When more substantial warm advection and deep upglide motion was present in these areas (typically ahead of *active* warm fronts), colder cloud tops and more significant precipitation often formed, but significant liquid water was still produced by the influx of warm, moist air. Clouds containing a mixture of snow and supercooled liquid water can occur in this scenario, especially if liquid production exceeds depletion by the ice crystals. The increased likelihood of partial or total depletion of SLW by snow may explain the lower threats for areas ahead of active warm fronts (8) compared to areas ahead of stationary warm fronts (48).

A layer of wind shear typically exists within the cloud deck near the warm frontal zone aloft. Pobanz et al. (1994) proposed that the existence of such a shear layer near the top of a predominantly liquid cloud was well correlated with the formation of large supercooled droplets. Recent work on WISP case studies has shown that shear within the cloud deck may also enhance the size of existing supercooled water droplets via the collision–coalescence process (Bernstein and Politovich 1996). These results are based on a relatively small sample of cases of shallow upslope flow in northeast Colorado and may not apply to warm fronts. Frequent observations of freezing precipitation at the surface within sectors 8 and 48 (Bernstein et al. 1997) support the concept that they are prime candidates for containing large supercooled liquid water droplets aloft.

Icing was more of a threat on the cold side than on the warm side of an active or stationary warm or arctic front. Icing threats tended to increase from sectors 5 to 8, 45 to 48, 14 to 12, and 54 to 52 (Fig. 5d). Relatively few icing PIREPS were found on the warm sides of these fronts, while more were found on the cold sides. The depth of the subfreezing, saturated layer in which icing could occur tended to increase as the depth of the cold air mass beneath the fronts increased; thus the threat of icing increased in this direction across the front.

The occurrence of dry air capping arctic fronts may be conducive to icing, since relatively high ($>-12°C$) cloud-top temperatures have a tendency to exist in these situations. Ice formation is often inefficient at such warm temperatures, so the clouds are more likely to contain supercooled liquid water. When warm, moist air masses ride over these fronts, deep cloud may result due to strong lifting and latent heat release, resulting in efficient ice formation and scavenging of any liquid. The fact that threats were higher behind stationary arctic fronts than behind active arctic fronts supports this idea, since weaker, more gradual lift tends to occur along stationary frontal boundaries, producing little chance for frontally driven convection and, thus, a better chance for supercooled water droplets to exist.

Notably large threats were also calculated for the main surface low pressure center (sector 18). Several combinations of cloud depth, temperature, and lift are likely to occur in this region, causing favorable environments for icing conditions to form. The areas on or behind surface troughs (19, 20) had above-average threats and were more conducive to icing than the areas ahead of troughs (21). Although the occluded low and front sectors (10, 23) had relatively high threats, occluded fronts and lows were few in number and small in size. Their areal extents were among the smallest of any sectors (Fig. 2b). Due to the lack of data on these sectors, it is not clear whether they were particularly conducive to icing.

The regions on and just behind drylines (sectors 2 and 3) were particularly free of icing conditions, due to their dry nature. Little convection formed along the drylines on the days studied. Of those sectors far from fronts, troughs, or low pressure centers (4, 9, 11, 15, and 25), only sector 9 (center of East Coast air masses) had 1 of the 10 highest threats calculated for worst or general icing, despite relatively high counts for some of the other large sectors. This is likely due to the lack of strong forcing near the surface in most of these sectors, and the greater propensity for weak orographic lift and saturated conditions to exist within sector 9.

By combining sectors into groups that represent certain portions of large-scale weather systems, an overview of the threats they present can be gained (see Table 4). These data indicate that areas near warm fronts (WRMSTA, WRMACT, WRMAHD1), especially 250–650 km ahead of both types of warm front (WRMAHD2), were the most likely places to encounter icing conditions. This was especially true for nearly all combinations of mixed and clear PIREPs, while trends for rime PIREPs were markedly weaker. The relatively high threats for moderate or greater intensity (5–8, all types) and worst PIREPs in warm frontal areas contradicts the work of Mason (1953a,b), which showed that warm frontal icing was typically trace to light in severity. Though much less of a threat than warm fronts, the areas ahead of active Pacific–continental cold fronts (PACAHD), within surface lows (LOWS) and along and immediately behind stationary and active arctic fronts (ARCON, ARCBHD) were more likely to be associated with icing conditions than average. Those sectors on and behind active and stationary warm fronts (WRMON, WRMBHD), ahead of arctic fronts (ARCAHD) and in the central portions of large air masses

TABLE 4. Threats (No. of PIREPs per 10^6 km^2) of several icing severity and/or icing type categories for combinations of cyclone sectors. Values are % different from threat calculated for all sectors combined (all). First three letters of sector combination indicate frontal type (ARC = arctic, OCC = occluded, PAC = Pacific, WRM = warm), remaining letters indicate location relative to front or frontal character (ON = on the front, AHD = ahead of the front, BHD = behind the front, STAT = stationary, ACT = active). Other combinations are explained in the text. Area is the total combined area for the sectors listed in the Sector column, which are those used in the calculations of threat for each row. Calculated threat for all sectors combined (all) is boldface.

		PIREP combinations (icing intensities and types indicated below)								
Sector combination	Sectors	5–8 Clear, mixed	5–8 Rime	1–8 All	5–8 All	7–8 All	1–8 Rime	1–8 Mixed	1–8 Clear	Area
All (threat)	**All**	**1.00**	**1.59**	**9.68**	**2.78**	**0.13**	**5.97**	**0.82**	**1.92**	**279.14**
WRMAHD2	8, 48	+606%	+348%	+339%	+464%	+523%	+265%	+621%	+409%	9.95
WRMSTA	45, 46, 47, 48	+350%	+171%	+196%	+259%	+286%	+139%	+435%	+221%	12.04
WRMACT	5, 6, 7, 8	+120%	+67%	+70%	+83%	+22%	+42%	+129%	+129%	12.75
WRMAHD1	7, 47	+76%	+10%	+36%	+32%	−100%	−6%	+49%	+101%	5.71
PACAHD	1, 41	+56%	+131%	+30%	+88%	+119%	+51%	−31%	+33%	7.08
LOWS	10, 18	+39%	+103%	+59%	+83%	+139%	+60%	+31%	+61%	6.49
TROUGHS	19, 20, 21	+37%	−8%	+8%	+7%	−61%	+2%	+10%	+29%	19.85
ARCON	13, 53	+21%	+38%	+47%	+46%	−15%	+43%	−7%	+60%	9.11
ARCBHD	12, 52	+20%	+45%	+44%	+32%	−42%	+45%	+9%	+67%	13.40
OCCFNT	22, 23, 24	+13%	+76%	+63%	+62%	−100%	+79%	−32%	−41%	1.78
ARCSTA	52, 53, 54	+11%	−7%	+1%	+9%	−15%	0%	−20%	+18%	18.16
ARCFNT	12, 13, 14, 52, 53, 54	−7%	+20%	+22%	+12%	−15%	+27%	−23%	+30%	36.56
WRMFNT	5, 6, 7, 45, 46, 47	−19%	−37%	−8%	−30%	−100%	−29%	+48%	+16%	14.84
ARCACT	12, 13, 14	−24%	+47%	+43%	+15%	−16%	+54%	−27%	+42%	18.40
PACFNT	1, 16, 17, 41, 56, 57	−25%	+37%	−10%	+10%	+94%	+11%	−70%	−22%	16.02
CENTERS	4, 9, 11, 15, 25	−32%	−25%	−23%	−29%	−20%	−19%	−27%	−31%	165.66
ARCAHD	14, 54	−50%	−15%	−15%	−28%	+10%	−1%	−65%	−26%	14.04
WRMON	6, 46	−73%	−100%	−10%	−90%	−100%	−25%	+126%	−31%	3.77
WRMBHD	5, 45	−81%	−41%	−54%	−53%	−100%	−56%	−9%	−42%	5.36

(CENTERS—far from fronts, troughs, and lows) were less likely to contain icing conditions than average.

Another important trend was that threats for worst PIREPs were notably higher for stationary warm (WRMSTA) and arctic (ARCSTA) fronts than for similar active fronts (WRMACT, ARCACT). This gives further evidence that relatively gradual, shallow lifting zones were more conducive to the most hazardous icing conditions. This trend was *reversed* for rime PIREPs near arctic fronts, with much higher threats for active rather than stationary Arctic fronts.

c. Precipitation type

The discussion of the relationship between PIREPs and either surface precipitation type or cloud cover cannot be conducted in terms of pure percentages. An individual PIREP could be matched to several precipitation types and cloud coverages, as opposed to a single airmass or cyclone sector. Thus, only the relative number of PIREP counts matched to and the threats calculated for each precipitation type will be presented. The precipitation types considered were rain (R), drizzle (L), snow (S), freezing rain (ZR), freezing drizzle (ZL), and ice pellets (IP). All subcategories of these precipitation types were included within them (e.g., snow, snow showers, snow grains, and snow pellets were all included in the S category, regardless of intensity). Nonprecipitation categories tested were no precipitation (NO), fog (F), and thunder (TH). The matching technique discussed in section 2 was used to create the statistics for precipitation type and cloud coverage.

Of those used in this study, 59% of general and 69% of worst PIREPs were associated with some form of precipitation at the surface. Of the precipitation types, most general PIREPs (Fig. 6a) were associated with S and R, while about one-third as many were associated with drizzle or the individual freezing precipitation types (ZL, ZR, and IP). Counts for occurrences of any freezing precipitation type matched to a PIREP (ZZ category) gave a total value that rivaled, but still fell short of, those for snow and rain. For worst PIREPs, counts for ZL and ZR were nearly equal to those for R, while counts for ZZ equaled those for S and were the highest of any precipitation type.

The high counts for snow and rain make little sense at first glance, since snow can scavenge SLW from clouds, and wintertime rain often forms via snow falling through a melting level. However, SLW can exist in separate layers from the snow or coexist with snow in clouds, if the production of SLW in the layer exceeds its depletion by snow. One reason for the high counts was the relatively large amount of areal coverage for S and R, compared to the other precipitation types (Fig. 2c). Snow and rain each covered more than 10×10^6 km^2, while all freezing precipitation types combined only covered 2.9×10^6 km^2. These large differences in areal coverage impacted the threats calculated for

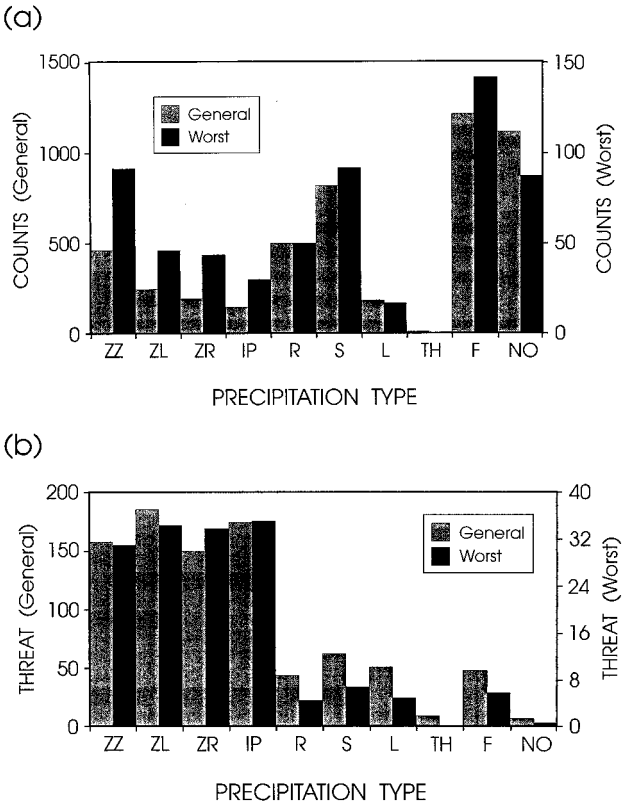

FIG. 6. (a) Number and (b) threats (counts/areal extents, PIREPs/10^6 km^2) of general (gray columns) and worst (black columns) PIREPs matched to precipitation types.

each precipitation type. Threats for ZL, ZR, and IP were about 2–4 times greater than those for R, S, and L for general PIREPs and 5–8 times greater for worst PIREPs (Fig. 6b).

Approximately 29% of general and 48% of worst PIREPs matched to any precipitation type occurred in an area of freezing precipitation. This result is significant since only 1% of the areal extent of the United States was covered with freezing precipitation during this study.

The dramatically higher threats for the freezing precipitation types make intuitive sense, since their observation at the surface indicates that precipitation-sized supercooled liquid water droplets exist through some depth. Freezing drizzle droplets, in particular, have recently been shown to be extremely hazardous to aircraft (Sand et al. 1984; Politovich 1989; Marwitz et al. 1997). Under appropriate thermodynamic conditions, these droplets can form a bumpy glaze on the wings, well aft of deicing devices such as pneumatic boots and wing heaters, which are typically along the leading edge of wings. The recent crash of a turboprop cargo plane over Great Britain (Pike 1995) and data from the University of North Dakota Citation, which indicated a need to increase fuel consumption by 60% to maintain the ice-free performance of the aircraft (Jeck 1996), provide two examples of the hazard of flight in ZR conditions. Thomas and Marwitz (1995), on the other hand, reported no significant effect on the University of Wyoming King Air during two research flights through ZR. Though these aircraft encounters with ZR supply contradicting evidence, the PIREP data presented here suggest that surface reports of ZR indicate the existence of hazardous conditions aloft.

Although IP itself is not a hazard to aviation, since the water has reached a solid form at that point, IP is indicative of a layer of precipitation-sized supercooled liquid drops aloft. Such drops may have contained some unmelted ice and had adequate time at subfreezing temperatures for them to freeze into ice pellets (as in Hanesiak and Stewart 1995). Thus, observations of ZL, ZR, and IP at the surface all indicate that large supercooled droplets must exist through some depth. Some observations of PIREPs with R and L at the surface may be due to the existence of freezing precipitation aloft that reached above-freezing air upon approaching the surface (as in Stewart 1985).

Many reports were recorded above or within surface fog, but fog did not prove to be a good indicator of icing aloft. This result is probably due to the shallow nature of fog, its large areal extent, and the fact that it can form by processes (e.g., radiation) that have little direct relation to synoptic-scale weather features. The low number of PIREPs associated with thunder (TH) may have been partially due to pilot avoidance of convective areas, especially when SIGMETS (SIGnificant METeorological information) have been issued for them. Although one would expect that the low counts for PIREPs matched to TH was simply due to a lack of thunder occurrences during winter, there were nearly as many observations of TH (95) as there were of IP (127). Thunder covered essentially the same amount of area as IP, ZR, and ZL did, yet threats for IP, ZR and ZL were much higher than those for TH (see Figs. 2c, 6b).

d. Mixtures of precipitation type

The correlations between precipitation type and icing PIREPs drawn earlier must be considered carefully. The mere facts that 30% of the general PIREPs were matched to some form of snow, and that the greatest threats of icing were within freezing precipitation areas, do not tell the whole story. As mentioned earlier, conventional wisdom says that when snow is occurring at the surface, icing conditions are not as likely to be found aloft. The statistic above strongly contradicts this rule of thumb. These statistics were based on the observation of snow by *any* SAO within 75 km of the PIREP. An observation of snow may have occurred toward one edge of the 75-km-radius circle considered, while this circle enclosed several other precipitation types, indicating that the PIREP occurred in a precipitation transition zone (see example in Fig. 7). It is important to consider whether those PIREPs matched to snow (or any other precipi-

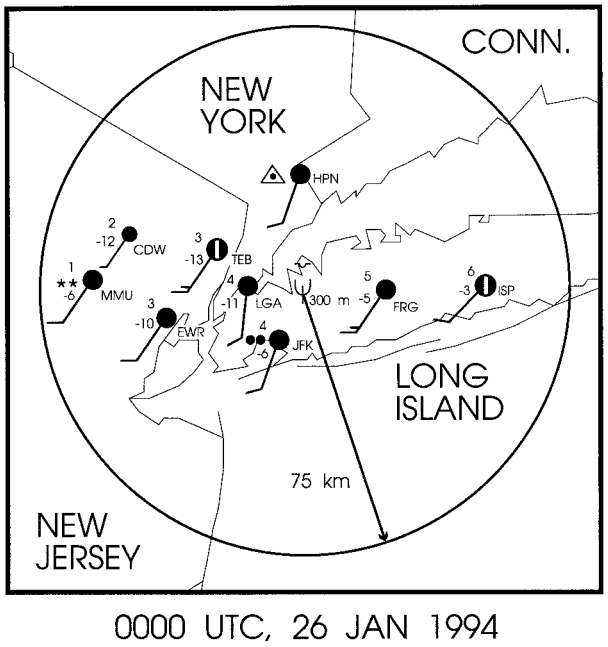

FIG. 7. Surface observations of precipitation type and intensity, with temperature, dewpoint (°C), wind barbs, and sky cover for SAOs within 75 km of a sample PIREP. Standard symbols are used for weather observations. Full wind barb = 5 m s^{-1}. Data are for 0000 26 January 1994.

tation type) were matched to that precipitation type *exclusively*, or if they were reported within a precipitation transition zone. The occurrence of some PIREPs in areas of the country where SAOs are more densely packed (e.g., near New York City) allowed for the possibility of more variation in reported precipitation type within the 75-km radius. However, more SAOs within the radius does not necessarily mean that more precipitation types will be matched to the PIREP.

Figure 8a graphically depicts the percentage of general PIREPs matched to a particular precipitation type that were matched to one or more precipitation types. On this plot, those PIREPs that fell within the ''one type'' category were exclusively matched to that precipitation type. In other words, that was the only precipitation type reported by SAOs within 75 km of the PIREP. The result that 70% of the general PIREPs matched to snow were found to be within regions that were exclusively snow is counterintuitive. This cannot simply be explained by assuming these PIREPs occurred within the nonprecipitating clouds that bordered on a snowfall region or snowbands, or by assuming those PIREPs occurred only above the portions of the 3-km depth where snow was occurring. It is possible that the snow was in the form of snow grains, snow pellets, and/or rimed snowflakes, all of which would indicate that liquid water was present in the cloud, and that the snow was scavenging the liquid via riming. In these cases, snow would have coexisted with the liquid water, possibly within the same cloud, and/or in separate layers

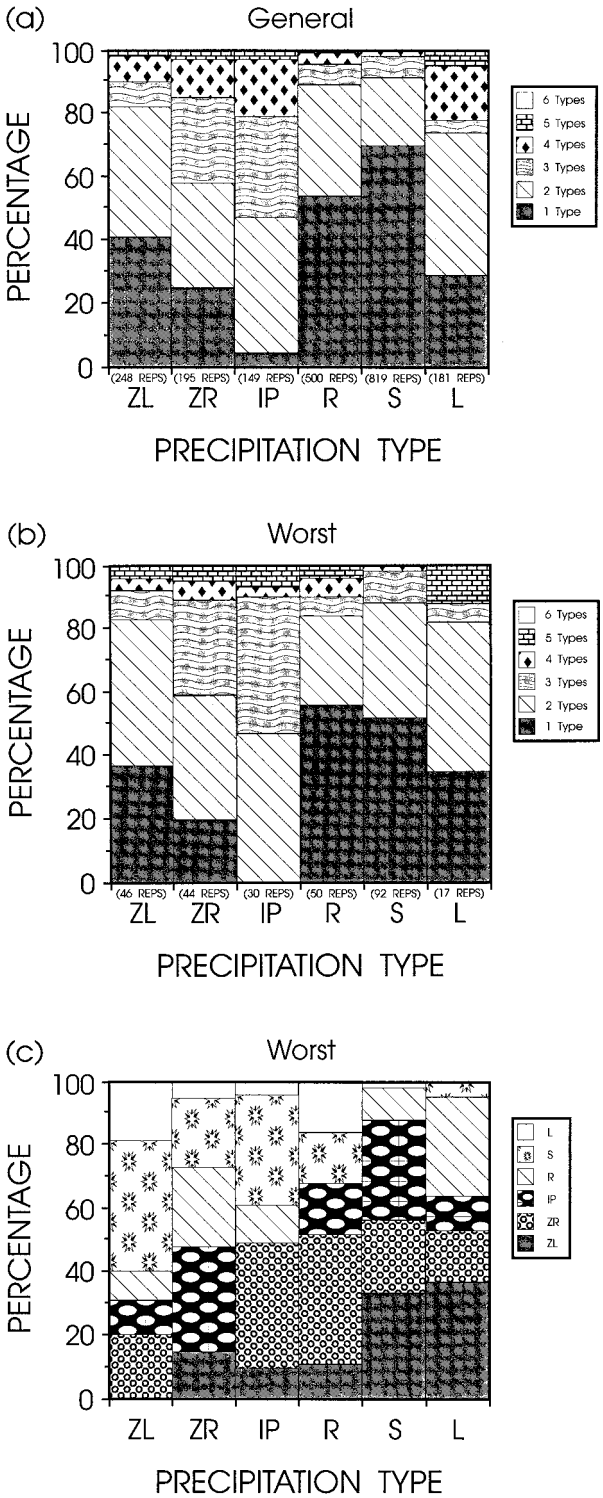

FIG. 8. Percentage of (a) general and (b) worst PIREPs matched with one to six different precipitation types for each precipitation category (ZL, ZR, IP, R, S, and L). Key for number of precipitation types that PIREPs were matched to is given on right side. (c) Percentage of WORST PIREPs matched to two or more precipitation types that were matched to each additional precipitation type. Key for precipitation type is given on right. Number of PIREPs (REPS) matched to each precipitation type is indicated.

(as in Rasmussen et al. 1995). It is likely that the combination of these possibilities explains the majority of those PIREPs matched exclusively to snow. A much smaller percentage of worst PIREPs (48%) were matched exclusively to snow, and ~88% of worst PIREPs matched to snow and another precipitation type were also matched to ZL, ZR, or IP, clearly indicating the existence of supercooled liquid water nearby (see Figs. 8b,c). Statistics calculated for rain were similar to those for snow. Since wintertime rain is typically formed via melting snow aloft, the arguments described for the PIREPs exclusively matched to snow are likely to also apply.

Results for the three freezing precipitation types are particularly interesting to compare. A much higher percentage of general and worst PIREPs were matched exclusively to ZL than exclusively to ZR or IP (Figs. 8a,b). This result is somewhat surprising since ZR tended to occur in larger swaths than ZL did, although it may be partially caused by the tendency for ZR to occur in transition zones. It appears that regions where only ZL was falling were more hazardous to aircraft than regions where only ZR was falling. Thus, although ZR was associated with a large number of PIREPs, 75%–80% of ZR matched PIREPs occurred in precipitation type transition zones. This was even more the case for IP PIREPs, of which <5% occurred within regions of exclusively IP. Regions where only IP was reported tended to be very small, since they often represented a narrow transition zone between freezing rain and snow (as in Stewart and King 1987; Hanesiak and Stewart 1995). Thus, by nature, there was almost always another precipitation type mixed in with the IP or being reported by a nearby station (Figs. 7, 8). These results compare well with anecdotal evidence from icing forecasters at AWC, which shows that icing PIREPs are not typically expected within regions dominated by SAOs reporting only ZR, but are more likely in areas where only ZL was reported and precipitation transition zones that include ZR and or IP (R. Olson, AWC, 1996, personal communication).

e. Cloud cover

Approximately 41% of General PIREPs occurred where no precipitation was falling at the surface (NO in Fig. 6a). Of those PIREPs not matched to any precipitation, most were matched to SAOs reporting overcast (OVC) conditions at some level (Fig. 9a). A gradual decrease in the number of PIREPs was observed with decreasing cloud cover. The exception to this trend was obscured sky conditions (XOB), which was matched to a relatively small number of PIREPs. Figure 2d indicates that this small count is likely attributable to the very small areal coverage of XOB conditions when no precipitation was occurring. All other cloud groups had areal coverage more than 20 times as large. The number of reports matched to XOB conditions was fairly large, however (255 PIREPs).

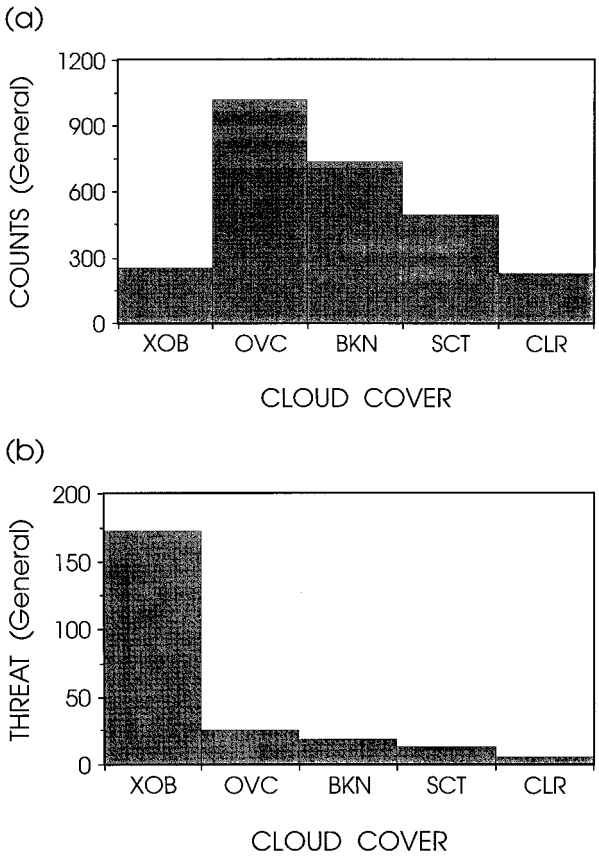

FIG. 9. (a) Number and (b) threat (PIREPs/10^6 km^2) of general PIREPs for all altitudes matched to each cloud cover.

Threats for cloud cover (Fig. 9b) overwhelmingly indicated that among nonprecipitating areas, those with obscured sky conditions were by far most likely to contain icing conditions. Threats were more than 7 times greater for XOB than for any other cloud cover. Overcast conditions came in a distant second, but OVC threats were 28% and 82% greater than those for BKN and SCT sky conditions, respectively. The fact that clear-sky conditions had any counts is likely attributable to the inclusion of automated weather station data, as described in section 2e, or errors in pilot-reported latitude and/or longitude. This explanation may also apply to a portion of the SCT and possibly BKN observations, but it is possible that discontinuous cloud can cause icing. Also, highly variable sky conditions could have easily existed within 75 km of a PIREP that occurred near a sharp transition zone, such as an arctic cold front, where even clear skies can precede postfrontal overcast skies and precipitation.

f. Icing events and forcing mechanisms

Icing event statistics further substantiate the results for PIREP counts, percentages, and threats described

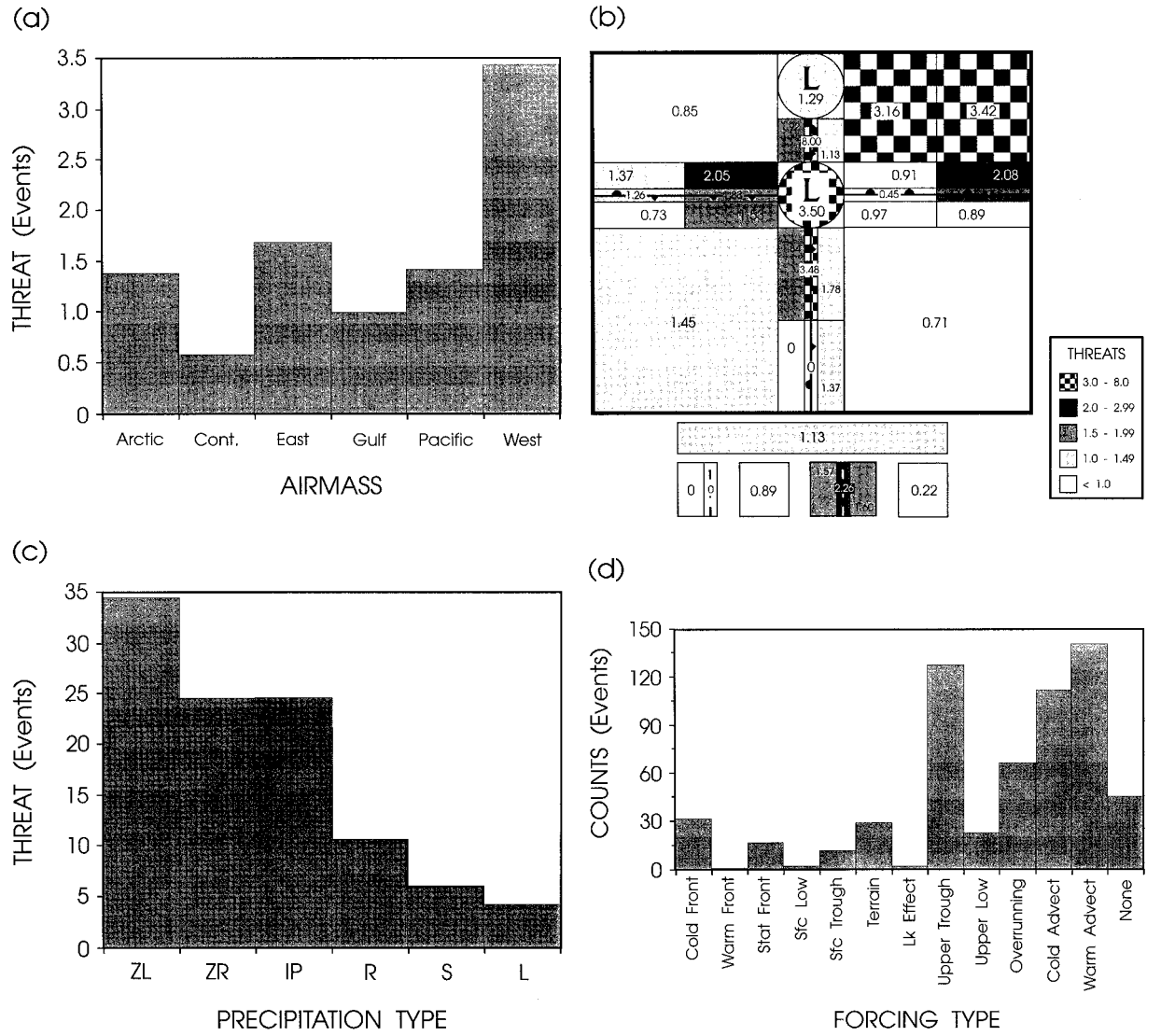

FIG. 10. Threats (No. of events/areal extent, events/10^6 km^2) of icing events for each (a) air mass, (b) cyclone sector, and (c) precipitation type. (d) Number of icing events matched to each synoptic-scale forcing mechanism. Cyclone sector key is given in Fig. 5a. Forcing mechanisms and are described in Table 2c.

above, as well as establish which forcing mechanisms were most frequently associated with icing. Forcing mechanisms could only be speculated on in earlier sections by discussing the meteorology often related to the surface air masses, sectors, precipitation types, and cloud cover. A total of 308 icing events were analyzed for this study. PIREPs from all altitudes were included in these events since the events were matched to weather features from the surface to 500 mb.

Results for event counts versus airmass type (not shown) indicated that the largest proportion of icing events (45%) occurred within the arctic air masses, while 18% and 11% occurred within continental and pacific air masses, respectively. These numbers are remarkably similar to those for the general PIREPs (Fig. 4a). As expected with such results, threats calculated by dividing the number of events matched to a particular air mass by the overall size of the air mass were almost exactly like those for general PIREPs (Fig. 4b), with largest threats calculated for West Coast air masses (Fig. 10a).

Counts and threats calculated for cyclone sectors (Fig. 10b) were also similar to those for worst PIREPs (Fig. 5d), but some differences are apparent. Although warm-front sectors continued to have relatively high threats for icing events, the sectors around the main surface low (18) and along active Pacific/continental cold fronts (17) had threats that were essentially equal to those for 250–600 km ahead of active and stationary warm fronts (8, 48). These results differ slightly from those shown earlier. Although earlier calculated threats for sector 18 were well above average, those for sector 17 were below

average for both general and worst PIREPs. Relatively high threats found for the sectors along and near occluded fronts must be questioned, due to the small number of data points used in their calculation.

Event results for precipitation types closely matched those for general and worst PIREPs. All three freezing precipitation categories had the highest threats by factors of about 2–8 when compared to other precipitation types (see Fig. 10c). Freezing drizzle had the highest threat value, exceeding ZR and IP by ~40%.

The relationship between icing events and synoptic-scale forcing mechanisms reflects the trends for cyclone sectors. Up to two forces were identified for each icing event; thus, the cumulative percentages of icing events associated with the forces was 200%. The areal extents of these features could not be readily determined, however, so threats could not be calculated. More icing events occurred in regions of warm advection (46.1%), near upper-level troughs (41.8%), with cold advection (36.6%), and overrunning (21.8%) than other forcing mechanisms by at least a factor of 2 (see Fig. 10d). Forbes et al. (1993) found a similar distribution of icing ''episodes'' with ''large-scale weather regime,'' as warm advection was related to the highest number of episodes, followed by low-level convergence, cold pockets aloft, cold advection, and overrunning. Warm advection and overrunning conditions aloft were typically observed in the vicinity of, and especially on the cold side (ahead) of, warm fronts. This correlates well with the tendency for icing events to occur within sectors 8 and 48, as well as with freezing precipitation brought about by such forcing mechanisms.

Upper-level troughs in the 850-, 700-, and 500-mb height fields were the reflection aloft of surface low pressure centers, cold fronts, warm fronts, and troughs. They were associated with both cold and warm advection, as well as upward and downward vertical motion. For this study, the troughs were not individually defined as ''upper-level cold fronts,'' ''upper-level warm fronts,'' or ''upper-level wind shift lines'' (not related to a surface front), so a finer distinction could not be made. Their high frequency of occurrence with icing events supports earlier correlations between icing conditions and regions: 1) ahead of surface warm fronts (sectors 8 and 48, where an upper-level warm front would be), 2) behind surface cold fronts (sectors 12 and 52, where an upper-level cold front would be), 3) near surface low pressure centers (sector 18, where upper-level fronts and/or wind shift lines would be), and 4) along surface troughs (sectors 19–21, where an upper-level wind shift or front would be).

Finally, cold advection often occurred aloft behind cold fronts and upper-level troughs. High counts for cold advection concur well with above-average threats for sectors just behind arctic cold fronts (12, 52). The relative percentage of occurrence of the different forcing mechanisms with icing events can be misleading because certain types of forcing (e.g., cold advection) were relatively common and often covered 25%–50% of constant pressure level charts, while others (e.g., closed low aloft) tended to cover much smaller areas and did not occur on some days. The areal extent of overrunning regions was relatively small on most days, so the relatively high percentage for this mechanism indicates that icing conditions often existed where there was overrunning. Terrain-forced (upslope) icing was noted in only ~10% of cases but was often not recorded as one of the two forcing mechanisms when other obvious forcing mechanisms were present. Thus, the relative importance of terrain forcing is underestimated in this dataset.

Of the other synoptic features tested versus icing events, only cloud cover and lightning activity proved to have any strong statistical relationship to them. Cloud cover was observed for 100% of the events, including stray events, as would be expected. This gives additional confidence in the quality of the PIREP dataset. Only 11% of all icing events occurred in areas where lightning was indicated in the lightning network composite. However, lightning tended to cover a small portion of the country on any given date and pilots tend to avoid areas of strong convection. Thus, areas where lightning is observed probably present a significant icing hazard. The correlation between reflectivity of at least VIP level 1 ($\geq$18 dBZ_e) was weak, with VIP level 1 observed within 56% of all icing event polygons. In most cases the reflectivity was spotty, which may indicate that icing situations were not widespread, but in intermittent pockets between precipitation cores (as seen in Politovich and Bernstein 1995; Marwitz et al. 1997). Those cases with reflectivity $\geq$18 dBZ_e may also have occurred in areas of freezing rain, ice pellets, or heavily rimed snow. All of these precipitation types indicate the existence of supercooled liquid water aloft, yet could produce reflectivities $\geq$18 dBZ_e, given high enough number concentrations and particle sizes (as in Martner et al. 1993).

5. Summary and conclusions

For this study, icing PIREPs and events were matched to specific classes of surface airmass type, location relative to surface weather fronts, low pressure centers and troughs, precipitation type, cloud cover, synoptic-scale forcing mechanisms, lightning/thunder, and radar reflectivity. This was accomplished through detailed analysis of the operationally available 0000 UTC weather data, including PIREPs, NCEP surface and upper-air data, national radar mosaics, GOES visible satellite imagery, and daily snow cover maps.

Results indicate that most PIREPs were associated with 1) arctic air masses; 2) cyclone sectors that were located deep within arctic, Pacific, West Coast, and continental air masses, and 250–600 km ahead of active and stationary warm fronts; 3) snow or rain at the surface when precipitation was observed at the surface; and 4) overcast conditions when precipitation was not

observed. When counts were normalized by the areal extent of these regions, the locations with the highest threat of icing (number of PIREPs per unit area) were 1) arctic, and East and West Coast air masses; 2) 250–600 km ahead of active and stationary warm fronts; 3) freezing precipitation areas (ZL, ZR, and IP) when precipitation was observed at the surface; and 4) obscured sky condition areas when precipitation was not observed. These locations proved to be even more likely (relative to other areas) to be associated with the worst icing conditions (icing of moderate or greater severity that was clear or mixed in type).

Freezing precipitation was associated with 48% of worst and 29% of general PIREPs matched to any precipitation type, while only 1% of the United States was covered with freezing precipitation. The ZL-matched PIREPs occurred in areas where only ZL was observed more often than ZR- or IP-matched PIREPs occurred in areas where only ZR or IP was observed. The ZR and IP PIREPs tended to occur within precipitation type transition zones. Areas where only ZL is observed should be considered particularly hazardous to aircraft. The same is true for locations where any freezing precipitation type is mixed with other types of precipitation, including other freezing precipitation types. By definition, large supercooled water drops exceeding the FAR Part 25, Appendix C, icing certification envelope (FAA, 1974) will exist above these locations. No aircraft is certified to fly in these conditions.

PIREPs that occurred within areas where only snow was reported at the surface were quite common, and were likely due to the simultaneous existence of snow and supercooled liquid water or their existence in separate cloud layers. Surface precipitation and cloud reports can be combined with model output, sounding, radar, and satellite data to identify icing locations aloft (as in Bernstein 1996). To properly assess the location of a potentially hazardous environment for aircraft in flight, however, it is critical that surface observations of freezing precipitation and delineation of precipitation type be done correctly, including those observations made by automated weather stations.

Identification of locations where icing conditions tend to occur and quantification of the hazards presented by different precipitation types, cloud coverages, portions of weather systems, and large-scale forcing mechanisms is one step toward understanding the physical reasons behind the success or failure of icing analyses and forecasts. In the future, the datasets created for and the results of this study can be applied to many other aspects of icing research, including improvements to model-based icing diagnoses and forecasts.

Acknowledgments. Many thanks to Randy Bullock for his programming efforts, which made this study possible. Thanks also to Ron Olson of AWC, for his input regarding current operational icing forecasts, and to Greg Thompson, Barb Brown, Rita Roberts, and Roy Rasmussen for their useful comments and suggestions.

This research is sponsored by the National Science Foundation through an interagency agreement in response to requirements and funding by the Federal Aviation Administration's Aviation Weather Development Program. The views expressed are those of the authors and do not necessarily represent the official policy or position of the U.S. government.

REFERENCES

Air Weather Service 1980: Forecasters' guide on aircraft icing. Air Weather Service Rep. AWS/TR-80/001, 58 pp. [Available from U.S. Air Force, Scott AFB, IL 62225.]

Bernstein, B. C., 1996: A new technique for identifying locations where supercooled large droplets are likely to exist: The stovepipe algorithm. Preprints, *15th Conf. on Weather Analysis and Forecasting,* Norfolk VA, Amer. Meteor. Soc., 5–8.

——, and M. K. Politovich, 1996: Formation of freezing drizzle via shear-induced collision-coalescence near cloud base. Preprints, *12th Int. Conf. on Clouds and Precipitation,* Zurich, Switzerland, Int. Commision on Clouds and Precipitation, 109–112.

——, ——, T. A. Omeron, and F. McDonough, 1997: Surface weather features associated with freezing precipitation and severe in-flight aircraft icing. *Atmos. Res.,* in press.

Brown, B. G., T. L. Fowler, B. C. Bernstein, and G. S. Forbes, 1993: Use of pilot reports for verification of aircraft icing diagnoses and forecasts. Preprints, *Fifth Int. Conf. on Aviation Weather Systems,* Vienna, VA, Amer. Meteor. Soc., 277–281.

——, G. Thompson, R. T. Bruintjes, R. Bullock, and T. Kane, 1997: Intercomparison of in-flight icing algorithms: Part II. Statistical verification results. *Wea. Forecasting,* **12,** 890–914.

Cober, S. G., G. A. Isaac, and J. W. Strapp, 1995: Aircraft icing measurements in East Coast winter storms. *J. Appl. Meteor.,* **34,** 88–100.

FAA, 1974: Federal airworthiness regulations, Part 25: Airworthiness standards, transport category airplanes. 158 pp. [Available from Federal Aviation Administration, U.S. Government Printing Office, Washington, DC 20401.]

Forbes, G. S., Y. Hu, B. G. Brown, B. C. Bernstein, and M. K. Politovich, 1993: Examination of conditions in the proximity of pilot reports of icing during STORM-FEST. Preprints, *Fifth Int. Conf. on Aviation Weather Systems,* Vienna, VA, Amer. Meteor. Soc., 282–286.

Hanesiak, J. M., and R. E. Stewart, 1995: The mesoscale and microscale structure of a severe ice pellet storm. *Mon. Wea. Rev.,* **123,** 3144–3162.

Jeck, R. K., 1996: Representative values of icing-related variables aloft in freezing rain and freezing drizzle. *Proc. FAA Int. Conf. on Aircraft Icing,* Vol. II, Springfield, VA, Federal Aviation Administration, 57–67.

Lewis, W., 1951: Meteorological aspects of aircraft icing. *Compendium of Meteorology,* T. F. Malone, Ed., Amer. Meteor. Soc., 1197–1203.

Martner, B. E., J. B. Snider, R. J. Zamora, G. P. Byrd, T. A. Niziol, and P. I. Joe, 1993: A remote-sensing view of a freezing-rain storm. *Mon. Wea. Rev.,* **121,** 2562–2577.

Marwitz, J. D., M. K. Politovich, B. C. Bernstein, F. M. Ralph, P. J. Neiman, R. Ashenden, and J. F. Bresch, 1997: Meteorological conditions associated with the ATR-72 aircraft accident near Roselawn, Indiana, on 31 October 1994. *Bull. Amer. Meteor. Soc.,* **78,** 41–52.

Mason, D., 1953a: Aircraft and icing research—I. *Weather,* **8,** 243–246.

——, 1953b: Aircraft and icing research—II. *Weather,* **8,** 261–267.

McCann, D. W., 1997: Five ways to produce supercooled drizzle drops. Preprints, *Seventh Conf. on Aviation, Range, and Aero-*

space Meteorology, Long Beach, CA, Amer. Meteor. Soc., 94–99.

Messinger, F., Z. I. Janjic, S. Nickovic, D. Gavrilov, and D. G. Deaven, 1988: The step-mountain coordinate: Model description and performance for cases of Alpine lee cyclogenesis and for a case of Appalachian redevelopment. *Mon. Wea. Rev.,* **116,** 1493–1518.

Newhouse, H., 1991: The National Weather Service lighting program. Preprints, *Fourth Int. Conf. on Aviation Weather Systems,* Paris, France, Amer. Meteor. Soc., 274–277.

Pike, W. S., 1995: Extreme warm frontal icing on 25 February 1994 causes an aircraft accident near Uttoxeter. *Meteor. Appl.,* **2,** 273–279.

Pobanz, B. M., J. D. Marwitz, and M. K. Politovich, 1994: Conditions associated with large-drop regions. *J. Appl. Meteor.,* **33,** 1366–1372.

Politovich, M. K., 1989: Aircraft icing caused by large supercooled droplets. *J. Appl. Meteor.,* **28,** 856–868.

——, 1996: Effect of icing on a research aircraft and evaluation of a severity index. *J. Aircraft.,* **33,** 291–297.

——, and R. Olson, 1991: An evaluation of aircraft icing forecasts for the continental United States. Preprints *Fourth Int. Conf. on Aviation Weather Systems,* Paris, France, Amer. Meteor. Soc., 234–238.

——, and B. C. Bernstein, 1995: Production and depletion of supercooled liquid water in a Colorado winter storm. *J. Appl. Meteor.,* **34,** 2631–2648.

Ramsay, A., 1996. Evaluation of the proposed ASOS freezing rain sensor. *Seventh Int., Workshop on Icing of Structures,* Chicoutimi, PQ, Canada, University of Quebec, 25–29.

Ranaudo, R. J., K. L. Mikkelsen, R. C. McKnight, and P. J. Perkins, 1984: Performance degradation of a typical twin engine commuter type aircraft in measured natural icing conditions. NASA Tech. Memo. 83564, 30 pp.

Rasmussen, R., and Coauthors, 1992: Winter Icing and Storms Project (WISP). *Bull. Amer. Meteor. Soc.,* **73,** 951–974.

——, B. C. Bernstein, M. Murakami, G. Stossmeister, J. Reisner, and B. Stankov, 1995: The 1990 Valentine's Day Arctic outbreak. Part I: Mesoscale and microscale structure and evolution of a Colorado Front Range shallow upslope cloud. *J. Appl. Meteor.,* **34,** 1481–1511.

Rutledge, S. A., and P. V. Hobbs, 1983: The mesoscale and microscale structure and organization of clouds and precipitation in midlatitude cyclones. VIII: Model for the seeder-feeder process in warm frontal rainbands. *J. Atmos. Sci.,* **40,** 1185–1206.

Sand, W. R., W. A. Cooper, M. K. Politovich, and D. L. Veal, 1984: Icing conditions encountered by a research aircraft. *J. Climate Appl. Meteor.,* **23,** 1427–1440.

Schultz, P., and M. K. Politovich, 1992: Toward the improvement of aircraft icing forecasts for the continental United States. *Wea. Forecasting,* **7,** 492–500.

Shin, J., B. Berkowitz, H. Chen, and T. Cebecci, 1991: Prediction of ice shapes and their effect on airfoil performance. NASA Tech. Memo. 103701, 22 pp.

Stewart, R. E., 1985: Precipitation types in winter storms. *Pure Appl. Geophys.,* **123,** 597–609.

——, 1991: Canadian Atlantic Storms Program: Progress and plans of the meteorological component. *Bull. Amer. Meteor. Soc.,* **72,** 364–371.

——, and P. King, 1987: Freezing precipitation in winter storms. *Mon. Wea. Rev.,* **115,** 1270–1279.

Thomas, M., and J. Marwitz, 1995: A procedure for inferring a detailed freezing rain sounding from NEXRAD and profiler data. Preprints, *27th Conf. on Radar Meteorology,* Vail, CO, Amer. Meteor. Soc., 351–352.